Available on the CERN CDS information server **CMS PAS HIG-16-007**

CMS Physics Analysis Summary

Contact: cms-pag-conveners-higgs@cern.ch 2016/03/29

Summary results of high mass BSM Higgs searches using CMS run-I data

The CMS Collaboration

Abstract

Exclusion contours are presented summarizing several searches for additional heavy Higgs bosons in physics models beyond the SM that have been performed with the CMS detector on the full LHC run-1 dataset collected during the years 2011 and 2012. The interpretation is restricted to two benchmark scenarios of the Two Higgs Doublet Model and two benchmark scenarios of the Minimal Supersymmetric SM.

1 Introduction

The physics program of the LHC run-1 data taking period during 2011 and 2012 has been most strikingly affected by the discovery of a new particle, with an invariant mass of 125 GeV by the ATLAS and CMS collaborations [1–5]. The discovery has been made at consistent values of the hypothesized invariant mass of the final state products in the ZZ [6, 7] and $\gamma\gamma$ [8, 9] final states, with convincing evidence in the WW [10, 11] and $\tau\tau$ [12–14] decay channels. The observation in the bosonic final states gives proof to the bosonic nature of the new particle. The evidence in the $\tau\tau$ final state, together with the non-observation in the $\mu\mu$ decay channel [15, 16] demonstrates a non-universal coupling of the new particle to fermions. Finally a detailed analysis of the spin, CP and decay width of the new particle [17–20] as well as a comprehensive analysis of its coupling structure [21–23] have revealed consistency with the expectations for the SM Higgs boson within $\mathcal{O}(10\%)$ precision. In particular the observed proportionality of the coupling to the mass of the fermions and to the mass squared of the vector bosons matches the SM expectation. The mass of the new particle has been measured to be $125.09 \pm 0.21(\text{stat.}) \pm 0.11(\text{syst.})$ GeV by combining the ATLAS and CMS analyses in the $\gamma\gamma$ and ZZ decay modes as these provide the best mass resolution [24]. In the following the observed Higgs boson will be referred to as H^0.

The search for the SM Higgs boson is not the only part of the Higgs physics program of the LHC experiments. A rich program of searches for (additional) Higgs bosons has been carried out by both experiments. In this note the results of several searches for additional heavy Higgs bosons in models beyond the SM are summarized that have been performed with data recorded by the CMS detector. The analyzed data correspond to the full LHC run-1 dataset collected during 2011 and 2012. It amounts to integrated luminosities between $19.7 - 24.8$ fb^{-1}. The results are shown in the form of exclusion contours in four benchmark scenarios. Two benchmark scenarios have been chosen within the *Two Higgs Doublet Model* (2HDM). The other two benchmark scenarios are defined within the *Minimal Supersymmetric SM* (MSSM). The shown exclusion contours are restricted to those analyses which contribute to a common parameter space of these scenarios.

Common to all considered scenarios is the presence of two $SU(2)_L$ doublet fields that can acquire a non-zero vacuum expectation value (VEV). As a consequence in contrast to the SM, they predict the presence of five Higgs bosons, of which three (h, H and A) are neutral and two ($H^\pm$) are charged. Of the neutral Higgs bosons the A is CP-odd, while the H and the h are CP-even. The latter are distinguished by their mass, h usually referring to the light and H to the heavy mass eigenstate of the mixing matrix, $\mathcal{M}^2$, of the two neutral CP-even Higgs boson states. In all considered scenarios the h is identified with the H^0. A constraint on all scenarios thus is that the h must be consistent with the observed mass and properties of the H^0. In particular the regularizing role of the Higgs sector in processes which otherwise violate unitarity, like vector boson scattering, together with the measured couplings of the H^0 impose strong constraints on the coupling strength of any additional Higgs boson.

In Section 2 the scenarios of choice are discussed in more detail. In Section 3 the data, for which exclusion contours are shown are summarized and the methods used to obtain the exclusion contours are discussed. The exclusion contours are given in Section 4.

2 Description of the 2HDM and MSSM scenarios

2.1 Description of the 2HDM scenarios

The most general 2HDM has many degrees of freedom yielding 14 a priori unconstrained parameters and four special *types*, depending on the way the two $SU(2)_L$ doublets are coupled to the fermion sector. For this note two 2HDM scenarios, one of *type*-I and and one of *type*-II have been chosen. In 2HDM's of *type*-I, the $SU(2)_L$ doublets couple to both *up*- and *down*-type fermions equally; in 2HDM's of *type*-II one doublet couples exclusively to *up*-type and the other exclusively to *down*-type fermions.

The 14 free parameters can be reduced to seven by the application of constraints on CP-violation (in the Higgs sector) and other external measurements. For the remaining seven parameters several possible basis choices can be made. A common choice that has been used for this note is the *physical basis*, in which the free parameters are the masses of the five physical Higgs bosons m_h, m_H, m_A and $m_{H^\pm}$, the mixing angle α of $\mathcal{M}^2$, the ratio of the vacuum expectation values of the two $SU(2)_L$ doublets, $\tan\beta$, and the soft $\mathbb{Z}_2$-breaking mass parameter m_{12}. The two angles α and β can be substituted by $\cos(\beta-\alpha)$ and $\tan\beta$ without loss of generality.

Two scenarios have been defined within the CMS collaboration to provide a parameter space that allows as many analyses to contribute to the summary exclusion plot as possible. The choice of parameters has been made equally for both scenarios, such that they differ only in their *type*. As will be discussed in Section 3, the couplings of the H^0 set already strong general constraints on $\cos(\beta-\alpha)$. For the scenarios considered here the value of $\cos(\beta-\alpha)$ has been fixed to 0.1, which is compatible with the constraints given by the couplings of the H^0 in most of the displayed parameter space. In this way the measured properties of the H^0 are manifestly incorporated into the definition of the scenarios.

For the 2HDM to fulfill perturbativity, unitarity, and vacuum stability, the masses of the remaining Higgs bosons should be roughly degenerate. However, in order to allow for the non-standard decay $A \to ZH$, m_A has been allowed to take values up to $m_A = m_{H^+} = m_H + 100$ GeV. Recent theoretical studies [25] have shown that decays of type $A \to ZH$ have the potential of a smoking gun signature for 2HDM incarnations that can lead to a cosmological first order electroweak phase transition and thus explain the origin of the matter-antimatter asymmetry in our Universe.

Finally, the model definition is left with m_{12}. For $m_{12} = 0$, the $\mathbb{Z}_2$ symmetry is maintained and CP will always be conserved. However, in this case the vacuum of the 2HDM becomes non-stable already for moderate values and non-perturbative for low values of $\tan\beta$. On the other hand CP-conservation may also be satisfied for $m_{12} \neq 0$ for certain choices of the other parameters thus maintaining a theoretically viable model. Since all other parameters have already been fixed, in practice this implies that m_{12} must be chosen with care to maintain theoretical consistency. To accomplish this, the decision has been made to follow the method of the *hybrid basis* described in Ref. [26], which guarantees theoretical consistency over a wide range of the 2HDM parameter space. For this purpose the physical masses have been translated from the *physical basis* into the *hybrid basis* and then solved for m_{12} at each point in the m_H–$\tan\beta$ plane. This procedure results in the following equations:

Table 1: Parameters of the 2HDM *type*-I and II scenarios used in this note. The parameters m_H and $\tan\beta$ are chosen for a 2-dimensional scan. The H^0 is interpreted as the h. The values of m_h and $\cos(\beta-\alpha)$ are then constrained by the measured properties of the H^0. The values of m_A and $m_{H^\pm}$ are taken to be degenerate and larger than m_H to allow for decays like $A \to ZH$. The only remaining parameter, m_{12}, then needs to be carefully chosen to guarantee vacuum stability and perturbativity of the model. This choice has partially been made in the 2HDM *hybrid basis* as referred to in the text.

Parameter	Value (type I or type II)
m_h	125.09 GeV
m_A	$m_H + 100$ GeV
m_{H^+}	$m_H + 100$ GeV
$\cos(\beta-\alpha)$	0.1
m_{12}^2	$\max(1-\tan\beta^{-2}, 0) \cdot \frac{1}{2}\sin(2\beta)(m_A^2 + \lambda_5 v^2)$
	m_H and $\tan\beta$ scanned.

$$
\begin{aligned}
m_{12}^2 &= \frac{1}{2}\sin(2\beta)(m_A^2 + \lambda_5 v^2) \\
\lambda_5 &= Z_5 + \frac{1}{2} Z_6 \tan(2\beta) \\
Z_5 &= \left[m_H^2 \sin(\beta-\alpha)^2 + m_h^2 \cos(\beta-\alpha)^2 - m_A^2\right] / v^2 \\
Z_6 &= \left[(m_h^2 - m_H^2)\cos(\beta-\alpha)\sin(\beta-\alpha)\right] / v^2 ,
\end{aligned}
\tag{1}
$$

where $v = 246.22$ GeV [27] corresponds to the VEV. However, this definition leads to a non-stable vacuum for low values of $\tan\beta$. Therefore the definition of the scenario has been modified for this region by letting m_{12} go to 0 for low values of $\tan\beta$, which brings the choice of m_{12} into its final form:

$$
m_{12}^2 = \max(1-\tan\beta^{-2}, 0) \cdot \frac{1}{2}\sin(2\beta)(m_A^2 + \lambda_5 v^2) , \tag{2}
$$

that defines the benchmark scenario for the 2HDM of both *types*. For the limit calculation cross sections and (partial) decay widths have been generated using the code `SusHi` [28] and `2HDMC` [29]. This has been done for a grid of several points in m_H and $\tan\beta$ to allow for 2-dimensional exclusion contours in these variables. A summary of all parameters is given in Table 1.

2.2 Description of the MSSM scenarios

The MSSM is a specific example of a 2HDM of *type*-II. The additional strong constraints given by the non-trivial fermion-boson symmetry fixes all mass relations between the Higgs bosons and the angle α, at tree-level, leaving only two free parameters to fully constrain the Higgs sector in the MSSM, instead of seven as in the general 2HDM case. In MSSM motivated searches for additional neutral Higgs bosons these two parameters are usually chosen to be m_A and $\tan\beta$.

The Higgs sector of the MSSM has been studied extensively already before the advent of the LHC. It has been exploited from the beginning of the LHC run-1 data taking period on, in the form of several benchmark scenarios [30], which were defined to match the experimental

observations within the uncertainties of the MSSM and to reveal characteristic features of certain regions of the parameter space. Based on this groundwork, for this note the m_h^{mod+} (with $\mu = +200$ GeV) and the $hMSSM$ scenario [31, 32] have been chosen. The m_h^{mod+} scenario is a modification of the former m_h^{max} scenario that had been defined to maximize the achievable values for m_h. In the m_h^{max} scenario m_h reached up to values of 130 GeV. After the discovery of the H^0 this scenario has been modified such that m_h is compatible with m_{H^0} within a theoretical uncertainty of ± 3 GeV [33] in as much of the parameter space as possible. The $hMSSM$ scenario has recently been introduced as an effective MSSM model, trading the precise knowledge of m_{H^0} against unknown higher order corrections in $\mathcal{M}^2$. In this way $m_h = m_{H^0}$ is again a manifest requirement of the scenario. This trade further allows one to obtain relatively simple relations between m_A, $\tan\beta$ and the anticipated SUSY modifications to the couplings to the h, as expected from the SM, as will be further discussed in Section 3. This scenario is strictly valid for $m_A > 130$ GeV and $\tan\beta < 10$. It can still be formulated for values up to $\tan\beta < 60$ though the omission of direct higher order SUSY corrections to *down*-type fermion couplings (also referred to as $\Delta\beta$ corrections) and corrections due to SUSY particles in loops, which become relevant for $\tan\beta > 10$ question the consistency of the predictions with SUSY. A detailed discussion of the $hMSSM$ has been given in Ref. [34].

3 Summary of the analyses entering the exclusion contours

3.1 Indirect constraints from the couplings of the H^0

When interpreted as the h the predicted production and decay rates of the H^0 are particularly sensitive to the angles α and β. In the 2HDM these angles are free parameters. In the $hMSSM$ they can be expressed in terms of the free parameters m_A and $\tan\beta$ [32]. Thus in both cases the allowed parameter space is constrained by the production and decay of the H^0.

Such constraints have been obtained using the CMS inputs to the combined ATLAS and CMS coupling analysis as presented in Ref. [23], for the $\gamma\gamma$, $ZZ(4\ell)$, $WW(2\ell 2\nu)$, $\tau\tau$ and bb decay channels. For the discussion within this note the existing data have been re-interpreted; the selected analyses have not been modified, in any other way. The production and decay rates of the h relative to the SM expectation have been varied using the formalism of leading order coupling modifiers, κ_i as defined in Ref. [35]. At leading order only three coupling modifiers are needed to capture the relevant modifications of h production and decay relative to the SM expectation in the considered scenarios. These are the modifiers for the coupling to *up*- and *down*-type fermions, κ_u and κ_d, and the coupling to vector bosons, κ_V. For convenience, the parameters $\lambda_{du} = \kappa_u/\kappa_d$, $\lambda_{Vu} = \kappa_V/\kappa_u$ and $\kappa_{uu} = \kappa_u^2/\kappa_h$ have been used, where κ_h (which can be calculated in terms of the coupling modifiers, κ_u, κ_d and κ_V, assuming only decays into SM particles) corresponds to the total width of the h, relative to the expectation of the SM. For the SM all parameters take the value 1.

Based on this model, in a first step a general 3-dimensional likelihood function $\mathcal{L}(\lambda_{du}, \lambda_{Vu}, \kappa_{uu})$ has been built. When maximized this likelihood function leads to the estimates $\hat{\lambda}_{du} = 1.008$, $\hat{\lambda}_{Vu} = 1.160$, $\hat{\kappa}_{uu} = 0.821$. For this and any further maximization, systematic uncertainties have been treated as nuisance parameters and profiled as done in the SM couplings analysis. The $\hat{\lambda}_i$ have been used in a log-likelihood scan of the form

$$q(\lambda_{du}, \lambda_{Vu}, \kappa_{uu}) = -2\ln\left(\frac{\mathcal{L}(\text{data}|\lambda_{du}, \lambda_{Vu}, \kappa_{uu})}{\mathcal{L}(\text{data}|\hat{\lambda}_{du}, \hat{\lambda}_{Vu}, \hat{\kappa}_{uu})}\right), \tag{3}$$

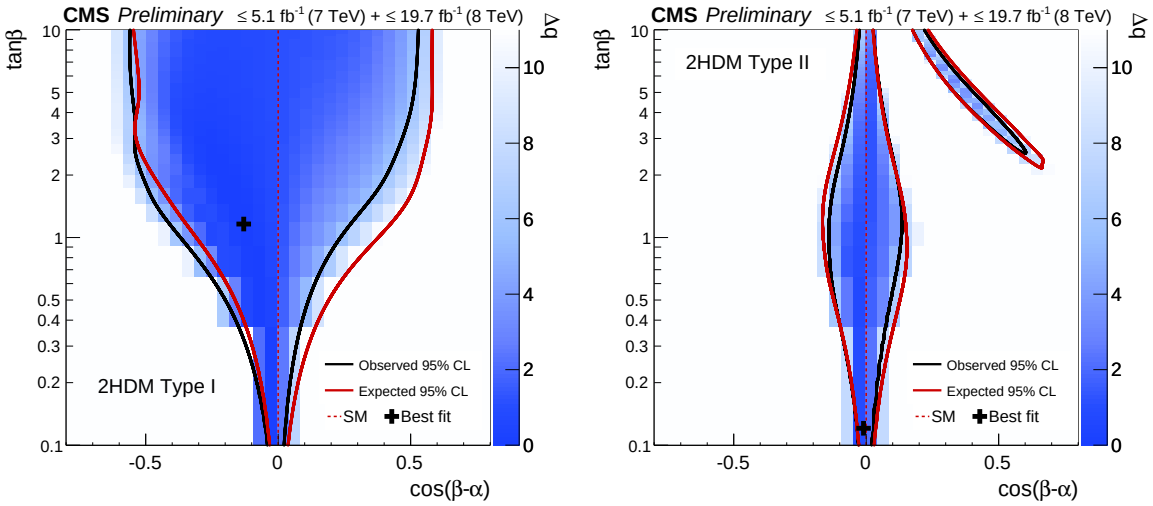

Figure 1: General constraints on the 2HDM parameter space obtained from the compatibility with the observed couplings of the H^0 when interpreted as the h. The lines show the contours which restrict the allowed parameter space at the 95% CL for a 2HDM of (left) *type*-I and (right) *type*-II. The contours have been obtained from an increase of the test statistic, $q(\cos(\beta-\alpha), \tan\beta)$, as defined in the text by $\Delta q = 5.99$ relative to the minimum in the $\cos(\beta-\alpha)$–$\tan\beta$ plane, corresponding to a 95% confidence region for a χ^2 function with two degrees of freedom. The observed constraints are shown in black. The expected constraints assuming just the SM Higgs sector are indicated by the red continuous line.

where the λ_i correspond to the points in a 3-dimensional grid. Under the 2HDM and the *hMSSM* scenario the λ_i are related reducing the dimensionality of $\mathcal{L}$ and q to a two-dimensional hyperplane in the space of $\{\lambda_i\}$: in the 2HDM the λ_i depend only on α and β, leading to a dependency that can be expressed as $q(\cos(\beta-\alpha), \tan\beta)$; in the *hMSSM* they depend on m_A and $\tan\beta$, leading to a dependency that can be expressed as $q(m_A, \tan\beta)$. The relations used for each scenario are given in Table 2.

The 95% CL exclusion contours in the 2HDM of *type*-I and II, as obtained from the observed couplings of the H^0, in the $\cos(\beta-\alpha)$–$\tan\beta$ plane, are shown in Figure 1 (left) and (right). The contours have been obtained from an increase of q, relative to the absolute minimum of $\Delta q = 5.99$, corresponding to a 95% confidence region for a χ^2 function with two degrees of freedom. The observed exclusion contours are shown in black. The expected exclusion contours, assuming only the SM Higgs sector, are indicated by the red continuous line. Also shown are the expectation by the SM (indicated by the red dashed line) and the likelihood estimate (indicated by the black cross).

In the 2HDM of *type*-I, small values of $\tan\beta$ produce large deviations in the absolute size of $\kappa_F = \kappa_u = \kappa_d$ except for the region around $\cos(\beta-\alpha) = 0$ (the alignment limit at which the SM Higgs couplings are obtained and the h is effectively decoupled from the rest of the Higgs sector). This can be understood from Table 2 (second column), where $\sin\beta \to 0$ will enhance any deviation from the SM couplings for $\cos\alpha \neq 0$. In the 2HDM of *type*-II, the same is true for κ_u. In addition for large values of $\tan\beta$ the coupling to *down*-type fermions takes large values as shown in Figure 1 (right). The constraints at low and high values of $\tan\beta$ are dominated by the constraints on the couplings of the h to the top-quark (largely through the top-quark loop in the gluon-fusion production process) and the τ, respectively. The small lobe observed at large $\tan\beta$ and $\cos(\beta-\alpha) > 0$ is due to the fact that κ_d is negative in this region while κ_u is positive.

Although the data slightly prefer a positive sign of λ_{du}, the positive and negative signs can not be distinguished at the 95% CL.

Note that these exclusions contours are general to all 2HDM's of these *types*. They thus apply to any further specified 2HDM scenario, as defined e.g. in Section 2. The Figure demonstrates that the observed couplings of the H^0 already set strong general constraints on the allowed values for $\cos(\beta-\alpha)$ for all 2HDM's of *type*-I or II. Values still allowed are $\cos(\beta-\alpha) \lesssim 0.5$ for the 2HDM of *type*-I and $\cos(\beta-\alpha) \lesssim 0.2$ for the 2HDM of *type*-II, which has been taken into account by the parameter choice for the 2HDM scenarios in Section 2. As can be seen from Figure 1 (right) the coupling constraint is stronger for the 2HDM of *type*-II. For this reason the exclusion summary plots for this scenario contain an additional 95% CL exclusion contour from the compatibility of the predicted couplings to the h with the observed couplings of the H^0 for values of $\tan\beta \gtrsim 2.5$. For this exclusion contour $\cos(\beta-\alpha) = 0.1$ has been fixed, according to the scenario, and only $\tan\beta$ has been varied as a free parameter in the scan. The exclusion contour has then been obtained from an increase of $q(\tan\beta)$, relative to the minimum in this parameter subspace, of $\Delta q = 3.84$, corresponding to a 95% CL confidence region for a χ^2 function with one degree of freedom. For the 2HDM scenario of *type*-I a similar scan yields an exclusion for $\tan\beta \gtrsim 0.5$, which coincides with the lower bound of the displayed parameter space.

Note that the coupling modifications for the 2HDM of *type*-II in Table 2 are identical to the tree-level modifications of the couplings of the h in the MSSM. In the $hMSSM$, which contains the additional constraint given by the exact knowledge of m_h, $\tan\alpha$ can be expressed by m_Z, m_h, m_A and $\tan\beta$. In this case the coupling modifications as given in Table 2 are completed by the relations for s_u and s_d given by

$$s_u = \frac{1}{\sqrt{1+\frac{(m_A^2+m_Z^2)^2\tan^2\beta}{(m_Z^2+m_A^2\tan^2\beta-m_h^2(1+\tan^2\beta))^2}}} \qquad s_d = s_u \cdot \frac{m_A^2+m_Z^2\tan\beta}{m_Z^2+m_A^2\tan^2\beta-m_h^2(1+\tan^2\beta)}\,, \tag{4}$$

where m_Z has been set to 91 GeV and m_A and $\tan\beta$ are subject to the parameter scan. These relations thus allow for a 95% CL exclusion as a function of m_A and $\tan\beta$ also in the summary exclusion plot for the $hMSSM$, which in this case has been obtained again from an increase of $q(m_A, \tan\beta)$, relative to the absolute minimum in the m_A–$\tan\beta$ plane, of $\Delta q = 5.99$, corresponding to a 95% confidence region for a χ^2 function with two degrees of freedom. An overview of the scenarios in which the coupling constraint will explicitly appear in the exclusion summary plot is given in Table 3.

3.2 Constraints from direct searches

In addition to the constraints from the coupling structure of the H^0 several direct searches for (additional heavy) Higgs bosons that have been published using the LHC run-1 dataset, contribute to the summary exclusion plots presented in this note. No indications for a signal have been observed in any of these searches and 95% CL limits have been set using the modified frequentist approach as used for the SM Higgs boson searches and described in Ref. [36, 37]. For the statistical inference uncertainties have been incorporated into the likelihood function in the form of nuisance parameters θ_i. There are two ways in which the limits have been obtained: (i) in a first way templates have been obtained for the full signal prediction for each value in the exclusion plane of the considered scenario (m_A–$\tan\beta$ in the MSSM or m_H–$\tan\beta$ in the 2HDM). These may contain the signal for a charged or up to three neutral Higgs bosons. With these

Table 2: Modifications of the couplings of the h to *up*- (κ_u), *down*-type (κ_d) fermions and vector bosons (κ_V), with respect to the SM expectation, in 2HDM's model of *type*-I (second column) and II (third column) and for the *hMSSM* (fourth column). The coupling modifications for the *hMSSM* are completed by the expressions for s_u and s_d as given in Equation (4).

	2HDM		**hMSSM**
	type I	type II/MSSM	
κ_V	$\sin(\beta-\alpha)$	$\sin(\beta-\alpha)$	$\frac{s_d+s_u\tan\beta}{\sqrt{1+\tan^2\beta}}$
κ_u	$\cos(\alpha)/\sin(\beta)$	$\cos(\alpha)/\sin(\beta)$	$s_u\frac{\sqrt{1+\tan^2\beta}}{\tan\beta}$
κ_d	$\cos(\alpha)/\sin(\beta)$	$-\sin(\alpha)/\cos(\beta)$	$s_d\sqrt{1+\tan^2\beta}$

templates the CL_S value is obtained for each point in the exclusion plane, based on a likelihood ratio

$$q(m_{A,H},\tan\beta)=\frac{\mathcal{L}(\text{data}|\mu\cdot s+b,\{\hat{\theta}_{i,\mu}\})\big|_{\mu=1}}{\mathcal{L}(\text{data}|\hat{\mu}\cdot s+b,\{\hat{\theta}_i\})}\,, \tag{5}$$

where μ corresponds to a single signal strength parameter, s to the expected signal and b to the expected background yields. The value $\mu=1$ corresponds to the exact prediction of the scenario for given $m_{A,H}$ and $\tan\beta$. The parameters $\{\hat{\theta}_{i,\mu}\}$ correspond to the best estimates of the nuisance parameters for a fixed value of μ, and $\{\hat{\theta}_i\}$ to the global best estimates of the nuisance parameters for $0\leq\hat{\mu}\leq 1$. Those points where CL_S falls below 0.05 are excluded at 95% CL. This method has been used for the $A/H/h\to\tau\tau$ (with a slightly different test statistic as discussed below), $A/H/h\to\mu\mu$ and the combined $A\to Zh(\ell\ell\tau\tau)$ and $H\to hh(bb\tau\tau)$ searches described below; (ii) in a second approach model-independent 95% CL limits have been obtained on the cross section times branching fraction of a single, narrow-width resonance (with the exception of the $H\to WW/ZZ$ analysis that takes the decay width of the H into account). These limits have been translated into the exclusion plane of each considered scenario by a comparison with the predicted cross section times branching fraction. This method has been used for all other analyses that are described below.

The following analyses that have been chosen for the summary exclusion plots have been published as searches for additional Higgs bosons in the context of the MSSM:

- A search in the $A/H/h\to\tau\tau$ channel [38], in a mass range from 90 to 1000 GeV. This is the most sensitive CMS search to all three neutral Higgs bosons in the MSSM. The discriminating variable is the fully reconstructed invariant di-τ mass, $m_{\tau\tau}$. The search is performed in the $\mu\mu$, $e\mu$, $\mu\tau_h$, $e\tau_h$ and $\tau_h\tau_h$ final states taking the subsequent decays of the τ into electrons, muons and hadrons into account and indicating the decay of the τ into hadrons by τ_h. Due to the presence of neutrinos in the decay of the di-τ system the invariant mass reconstruction is further complicated, which is addressed by a likelihood based reconstruction method [39]. The resolution that can be achieved ranges between 10–20% of $m_{\tau\tau}$, depending on the final state. To increase the sensitivity of the analysis to the MSSM, event categories are exploited that take advantage of the predicted increased production of the A and the H in association with b-quarks, due to the enhanced coupling to *down*-type fermions. For the limit setting the coarse experimental resolution of $m_{\tau\tau}$ justifies the use of single mass templates obtained from the simulation with `Pythia` [40], which have been

produced for 14 different values in m_A. These templates are interpolated to the predicted masses for each corresponding Higgs boson (h, H or A), using horizontal histogram morphing techniques [41], and scaled to the prediction of the cross section times branching fraction for given m_A and $\tan\beta$ in the corresponding scenario. The templates that have been obtained in this way are added to result in the final prediction. Since this analysis is the only one among the searches in the context of the MSSM with a realistic sensitivity to the H^0 a test statistic with the null-hypothesis of a single SM-like resonance at 125 GeV and the MSSM signal hypothesis is used.

- A search in the $A/H/h \to \mu\mu$ channel [42], in a mass range from 115 to 300 GeV. This analysis is performed as a classical search for resonances in the di-μ invariant mass, exploiting the excellent di-μ mass resolution of the CMS detector, of 1–2%. To increase the sensitivity to the MSSM the events are split into an event category sensitive to the production in association with b-quarks and an event category targeting the normal production via gluon fusion, similar to the analysis in the di-τ final state. The fact that the reconstructed invariant di-μ mass is sensitive to the exact decay widths of the Higgs bosons requires the production of a full model prediction for each value in m_A and $\tan\beta$. This has been obtained by simulation, using `Pythia` provided with the predictions for all three neutral Higgs bosons as obtained from `FeynHiggs` [33, 43–46], on a grid of 324 points. The obtained templates have been fitted by a parametrization, which has been checked to describe all templates at the same time. In the following analysis this parametrization is then used to obtain the model predictions with the high mass resolution required by the final state.
- A search in the $A/H \to bb$ channel [47], in a mass range from 100 to 900 GeV. For sensitivity reasons, this analysis is restricted to the search only for the heavy Higgs bosons, A and H, and the production in association with b-quarks, leading to an event signature with large b-jet multiplicity. The discriminating variables in the analysis are the invariant mass of the two leading b-jets, m_{bb}, and an event variable for the presence and quality of secondary vertices after an event selection of at least three jets passing a tight b-tag requirement. The m_{bb} resolution is about 20%. In the lack of sensitivity to the h, model-independent limits are set on the cross section times branching fraction of a single resonance decaying into b-quarks for the production in association with b-quarks. Since in the MSSM at high values of $\tan\beta$ the A and the H are degenerate in mass a potential signal can be interpreted as the incoherent sum of these two individual contributions. The obtained limit is then translated into an exclusion contour for the corresponding MSSM scenario comparing the predicted production cross sections and branching fractions to the model independent limits.
- A search for charged Higgs bosons ($H^\pm \to \tau\nu$) [48] in the $\tau\nu$ and tb final states. In the kinematic phasespace available in the LHC run-1 data taking period, the sensitivity of this search is by far dominated by the $\tau\nu$ final state. The analysis is split in two distinct kinematic regions: (i) a low mass search (for 80 GeV $< m_{H^+} <$ 160 GeV) targets $H^\pm$ production via SM $t\bar{t}$ production, in which the $H^\pm$ is radiated off from one of the two top-quarks; (ii) a high mass search (for 180 GeV $< m_{H^+} <$ 600 GeV) exploits $H^\pm$ production in association with top-quarks. The intermediate mass range of $m_{H^\pm} \approx m_t$ where both processes contribute is not covered since their interference adds further complication to the theoretical predictions, which are not available for this reason. The analysis in the $\tau\nu$ final state is restricted to 'one-prong' hadronic τ decays to suppress background from QCD multijet production. The discriminating variable is the transverse mass distribution calculated from the visible part of the τ_h

and the reconstructed missing energy in each selected event. Limits are determined as a function of $m_{H^\pm}$ and $\tan\beta$, which, for the summary exclusion plot are then been translated into the m_A–$\tan\beta$ exclusion plane using the predicted mass relations of the m_h^{mod+} scenario.

- An MSSM motivated combined search for $H \to hh(bb\tau\tau)$ and $A \to Zh(\ell\ell\tau\tau)$ decays [49] in a mass range from 220 to 350 GeV. These decays gained interest due to the large number of mass constraints in the decay chain. In the MSSM they achieve sensitivity in the low $\tan\beta$ region for $m_A < 2m_t$. In the $A \to Zh$ channel the Z boson is required subsequently to decay into leptons and the h into τ's. In the $H \to hh(bb\tau\tau)$ decay channel one h has been required to decay into τ's and the other one into b-quarks. In both decay channels the reconstructed final state objects are required to lie within a window of the invariant mass of the corresponding intermediate boson in the decay chain. The discriminating variable is the fully reconstructed mass of the heavy Higgs boson (A or H respectively) from all accessible final state objects in the detector, after an additional kinematic fit in the $H \to hh(bb\tau\tau)$ decay channel. The limit of the combined analysis is largely driven by the $A \to Zh(\ell\ell\tau\tau)$ decay.

In addition the following searches for (additional heavy) Higgs bosons, which were not originally MSSM motivated, have been added to the summary exclusion plots of this note:

- A search for $H \to hh(bb\gamma\gamma)$ decays [50] in a mass range from 260 to 1100 GeV. One h is required subsequently to decay into b-quarks and the other one into photons. In contrast to the analysis in the $bb\tau\tau$ final state this analysis has a wider and more model independent scope. For the signal a radion model is chosen as a proxy. In a mass range of $260 \leq m_H \leq 400$ GeV, relevant for the summary exclusion plots shown in this note, a two dimensional unbinned fit is used for the signal extraction, exploiting the line-shape of both h bosons (making particular use of the excellent $m_{\gamma\gamma}$ resolution of the CMS detector), where the selected events are required to lie in a four body mass window around the H candidate mass. Model-independent limits have been set for this search that are re-interpreted in the corresponding scenarios for this note.
- A general search for an additional heavy Higgs boson, $H \to WW/ZZ$, in a mass range between 145 GeV and 1000 GeV [51]. This analysis is performed in a combination of 55 event categories in the WW and ZZ final states $WW(2\ell 2\nu)$, $WW(2\ell 2q)$, $ZZ(4\ell)$, $ZZ(2\ell 2\nu)$, $ZZ(2\ell 2q)$. The analysis is performed as a peak search in the invariant di-boson mass in each sub-decay channel. The mass resolution of each sub-decay channel varies between 20% (in $WW(2\ell 2\nu)$) and 1-2% (in $ZZ(4\ell)$). Model-independent limits are set also for this search, for different hypotheses on the decay width of the signal, that are re-interpreted in the corresponding scenarios of this note.
- A search for $A \to ZH$ decays [52] in a mass range from 140 to 1000 GeV in m_A. For the search the Z boson is required to subsequently decay into leptons and the H into b-quarks or τ's. In the $\ell\ell bb$ final state the discriminating variables are the invariant mass of the b-jets forming the H, m_{bb}, and the invariant mass reconstructed from the b-jets and leptons, $m_{\ell\ell bb}$ in a 2-dimensional shape analysis. In the $\ell\ell\tau\tau$ final state the discriminating variable is $m_{\tau\tau}$, which has been reconstructed using the same technique as described for the $A/H/h \to \tau\tau$ analysis. Limits have been set for this analysis that are re-interpreted in the corresponding scenarios for this note. The decay $A \to ZH$ is 2HDM specific. In the MSSM it is kinematically not allowed since the A and H are degenerate in mass, with $m_H \gtrsim m_A$. The definition of the 2HDM

Table 3: Summary of all published CMS analyses that have been used for the exclusion summary plots in the four scenarios presented in this note. The order corresponds to the order of appearance in the text, where each of the analyses is described in more detail. For those analyses indicated by a * the exclusion contours have been obtained directly from the publication. For those analyses indicated by a $^\bullet$ ($^\diamond$) the exclusion contours have been obtained extrapolating the published model independent 95% CL limits on the cross section times branching fraction to the scenarios presented here (or by a re-interpretation of the published results based on the existing likelihood model). More details are given in Section 3.2 in the text.

		2HDM		**MSSM**	
Constraint/Direct search		*type*-I	*type*-II	*hMSSM*	m_h^{mod+}
Couping constraint	[23]		☑$^\diamond$	☑$^\diamond$	
$A/H/h \to \tau\tau$	[38]	☑$^\diamond$	☑$^\diamond$	☑$^\diamond$	☑*
$A/H/h \to \mu\mu$	[42]			☑$^\bullet$	☑*
$A/H \to bb$	[47]			☑$^\bullet$	☑*
$H^\pm \to \tau\nu$	[48]				☑*
$H \to hh(bb\tau\tau)$ / $A \to Zh(\ell\ell\tau\tau)$	[49]			☑$^\diamond$	
$H \to hh(bb\gamma\gamma)$	[50]			☑$^\bullet$	
$H \to WW/ZZ$	[51]	☑$^\bullet$	☑$^\bullet$	☑$^\bullet$	☑$^\bullet$
$A \to ZH(\ell\ell\, bb)$	[52]	☑$^\bullet$	☑$^\bullet$		
$A \to ZH(\ell\ell\tau\tau)$	[52]	☑$^\bullet$	☑$^\bullet$		

benchmark scenarios has been made such that this special analysis contributes to the summary exclusion plots.

A summary of all direct searches that have been considered for the summary exclusion plots and to what scenarios they contribute is given in Table 3.

4 Discussion of summary exclusion plots

The 95% CL exclusion contours of the searches that contribute to the chosen parameter spaces in the four scenarios discussed in Section 2 are shown in Figures 2 and 3. The observed exclusion contours are indicated by the transparently filled areas in different colors, corresponding to the individual searches. The expected exclusion contours in the presence of a SM-like Higgs sector are shown in the same color as the observed ones (in a slightly darker shade) with a hatching to indicate the region of exclusion.

The exclusion contours for the 2HDM scenarios of *type*-I and II are shown in Figures 2 (left) and (right). In both cases the results are given for a range of $150 \leq m_H \leq 500$ GeV and $\tan\beta$ between 0.5 and 10. The gray shaded areas correspond to the regions where each corresponding scenario is either non-perturbative or unstable. As discussed in Sections 2 and 3, by definition the whole parameter space that is displayed is mostly compatible with the constraints imposed by the couplings of the H^0. For the *type*-II scenario, the additional constraint for $\tan\beta \gtrsim 2.5$ that is shown by the magenta colored area in Figure 2 (right) corresponds to the tighter constraint on $\cos(\beta-\alpha)$ in Figure 1 (right). In addition to this the exclusion contours of four direct searches are displayed for both scenarios: the (orange) $H \to WW/ZZ$ search shows a constant exclusion for $\tan\beta \lesssim 2$ for $200 \leq m_H \leq 360$ GeV, where the lower boundary in m_H marks the kinematically allowed region for decays into vector bosons and the upper boundary coincides with the opening of the decay into top-quarks. While the upper edge of the exclusion contour is quite sharp in both scenarios, the lower edge is more washed out with a slightly higher

sensitivity in the *type*-II scenario. The red (green) exclusion contours have been obtained from the search for $A \to ZH$ decays in the $\ell\ell bb$ ($\ell\ell\tau\tau$) final states. They both exclude a region of $m_H \lesssim 240$ GeV and $\tan\beta \lesssim 2.5$ in both scenarios, with a slightly further reach in m_H in the *type*-I scenario and a significantly further reach in $\tan\beta$ in the *type*-II scenario. The sharp edge of the exclusion contour for $m_H \lesssim 240$ GeV again coincides with the opening of the decay of the A into top-quarks. Note that these analyses have been performed as searches for the A and $m_A = m_H + 100$ GeV. In general both final states show the same exclusion behavior while the search in the $\ell\ell bb$ final state shows the larger expected exclusion range. The (blue) $A/H/h \to \tau\tau$ search shows a slightly different behavior between the two scenarios. For the *type*-I scenario for all three Higgs bosons the dominant contribution to the exclusion originates from the production via gluon fusion. The contribution of the production in association with b-quarks plays only a marginal role. The moderate rise for $m_H < 300$ GeV coincides with a rising cross section especially of the H. From $m_H > 300$ GeV on the exclusion contour flattens out. In this regime it is driven by the production cross section of the h. The constraint on the coupling of the H^0 to fermions (κ_f) is driven by the SM $H \to \tau\tau$ search. It leads to an exclusion right at the boundary of $\tan\beta \gtrsim 0.5$. The $A/H/h \to \tau\tau$ search of [38] has a similar sensitivity to the h for the production in gluon fusion compared to the SM $H \to \tau\tau$ search used for the analysis of the coupling constraint. In the re-interpretation of the result it is further supported by an additional though small contribution of signal from the production in association with b-quarks. Since the predicted rise of the cross section times branching fraction for this search for increasing $\tan\beta$ is relatively shallow (≈ 0.06 pb per unit in $\tan\beta$) these small differences lead to the fact the $A/H/h \to \tau\tau$ analysis can have a slightly stronger exclusion in $\tan\beta$ than the coupling constraint. In the *type*-II scenario the exclusion contours follow the trend of cross section times branching fraction for the A and the H. The higher exclusion sensitivity originates from the enhanced coupling of the A and the H to *down*-type fermions for increasing $\tan\beta$. In the combination of all direct searches and the coupling constraint the *type*-II scenario is excluded at 95% CL up to $m_H \approx 380$ GeV with a very small remaining corridor for values of $\tan\beta \approx 2$. The *type*-I scenario is less constrained.

The exclusion contours of five direct searches in the MSSM m_h^{mod+} scenarios are displayed in Figure 3 (left): the figure shows an exclusion up to $\tan\beta \approx 60$ for masses up to $m_A = 1$ TeV. For larger values of $\tan\beta$ the predictions in general turn unstable. Sticking to the classic searches for additional neutral Higgs bosons, in the doubly logarithmic presentation the excluded region decreases linearly down to values of $\tan\beta \approx 3$ (for $m_A \approx 140$ GeV), increasing again for lower values of m_A (up to values of $\tan\beta \approx 6$), since the most sensitive search, $A/H/h \to \tau\tau$ (shown in blue) is unable to separate signal and background due to the presence of $Z \to \tau\tau$ events with $m_Z \approx m_A$ in this case. [1] The strongest exclusion sensitivity for high values of m_A and $\tan\beta$ is reached for the $A/H/h \to \tau\tau$ search, supported by the independently obtained exclusion contours for the (cyan) $A/H \to bb$ and (yellow) $A/H/h \to \mu\mu$ searches. This behavior can be understood in terms of the coupling of the Higgs bosons being proportional to the mass of the final state particle (in the case of τ's and muons) and the difficulty to distinguish the signal from the overwhelmingly large background from QCD multijet production in the case of b-quarks.

For values of $m_A \lesssim 300$ GeV the $A/H/h \to \tau\tau$ search is sensitive to another rise of the overall predicted production cross section in the m_h^{mod+} scenario with a minimum for values of $\tan\beta \approx 3$. This minimum can be explained by two competing effects: (i) on the one hand the branching fraction to τ's decreases with decreasing $\tan\beta$, given by the tree-level relations be-

[1] For a Higgs signal around 90 GeV the shape analysis in the $A/H/h \to \tau\tau$ channel turns into a quasi counting experiment.

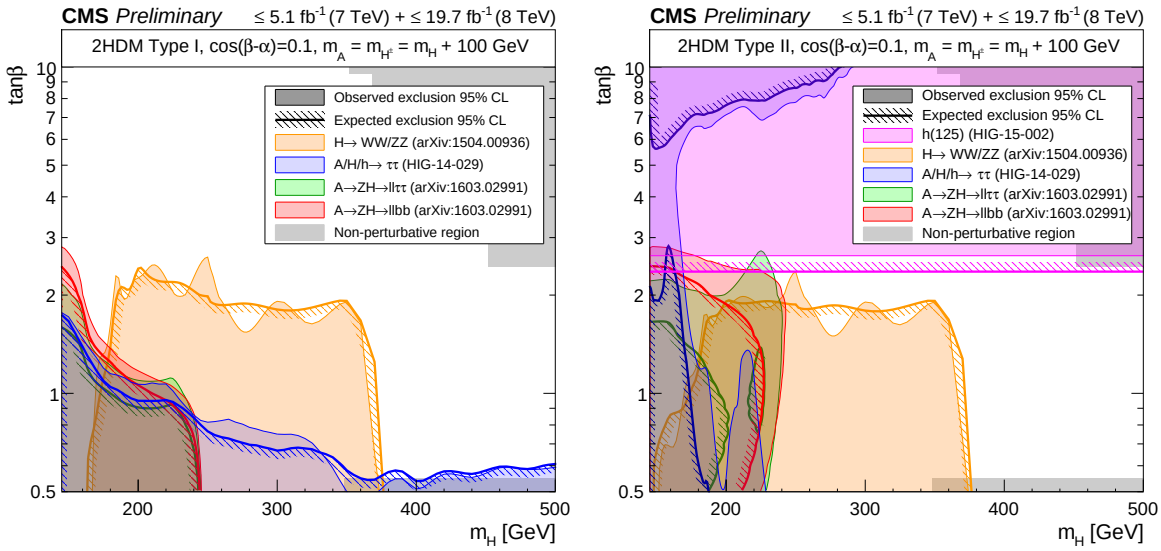

Figure 2: 95% CL exclusion contours, in two 2HDM scenarios of (left) *type*-I and (right) *type*-II, as obtained by selected CMS analyses that have been performed on the LHC run-1 dataset. The two scenarios have been defined in Table 1 and described in more detail in the text. The exclusion contours for all direct searches have been determined as CL_S limits or re-interpreted from such limits. The colored filled areas correspond to the excluded regions in m_H and $\tan\beta$. The colored (slightly darker shaded) lines with indicated hatches to the regions that were expected to be excluded, based on the null-hypothesis assumption of a SM-like Higgs sector. Those regions in m_H and $\tan\beta$ where the corresponding scenario is non-perturbative or unstable are marked in gray. In the figure on the right in addition to the direct exclusion contours the constraint is displayed that is obtained from the compatibility of the scenario with the couplings of the H^0. This constraint has been obtained from an increase of the test statistic, $q(\tan\beta)$, as defined in the text by $\Delta q = 3.84$, corresponding to a 95% confidence region of a χ^2 function for one degree of freedom.

tween the SM couplings and the MSSM e.g. as given in Table 2; (ii) on the other hand the cross section for gluon fusion is subject to negative tb-interference effects from the individual gluon fusion amplitudes with b- and top-quarks in the loop. These interference effects gain more importance the stronger the coupling to the b-quark becomes, i.e. with increasing values of $\tan\beta$. Since the interference term is negative the cross section will increase with decreasing $\tan\beta$. In consequence the predicted cross section for gluon fusion decreases with decreasing $\tan\beta$ due to (i) up to some turning point at $\tan\beta \approx 3$ and increases again due to (ii) for lower values of $\tan\beta$ beyond this point. At the same time the importance of the production in association with b-quarks decreases, so that the predicted cross section will be driven by gluon fusion. This explains the expected sensitivity of the $A/H/h \to \tau\tau$ search for low values of $\tan\beta$. Since the exact location of the cross section minimum depends on the exact kinematics (i.e. the value of m_A) and higher order QCD and SUSY corrections the region of $\tan\beta \lesssim 3$ is difficult to control theoretically, which explains the three localized areas of expected exclusion rather than a more continuous contour.

The $H^\pm \to \tau\nu$ analysis (shown in magenta) excludes over the whole range of $\tan\beta$ for $m_A < 160$ GeV, corresponding to the complete kinematic range of the low $m_{H^\pm}$ search. In the high $m_{H^\pm}$ search small areas of expected and observed exclusion are visible for very low and very high values of $\tan\beta$. The (orange) high mass $H \to WW/ZZ$ search leads to an exclusion for low values of m_A and $\tan\beta$, where the H-coupling to vector bosons allows for a significant branching fraction in the m_h^{mod+} scenario. For this analysis the limits on m_H have been translated into the m_A–$\tan\beta$ exclusion plane using the predicted mass relations of the m_h^{mod+} scenario. In general the H and the A are degenerate in mass. This is not the case any more for low values of $\tan\beta$, where m_H can be significantly larger than m_A. This causes the the expected limit that reaches to lower values of $\tan\beta$ also to reach to lower values in m_A in the exclusion contour.

In the m_h^{mod+} scenario m_h varies as a function of m_A and $\tan\beta$ leading to $m_h \approx 125$ GeV in the decoupling limit. But it can be significantly lower than m_{H^0} for lower values of m_A and $\tan\beta$. The theoretical uncertainty of the MSSM predictions on m_h has been estimated to be ± 3 GeV [33]. In addition to the individual exclusion contours the lines for five different values of m_h around 125 GeV have been added to the figure (as red dashed lines) to give an impression of the region of the scenario, which is compatible with m_{H^0} within these uncertainties. According to these limits the m_h^{mod+} scenario is severely constrained up to values of $m_A \gtrsim 300$ GeV (driven by the $A/H/h \to \tau\tau$ search and the constraint of m_{H^0}) and directly excluded for values up to $m_A \gtrsim 160$ GeV (again driven by the $A/H/h \to \tau\tau$ and the $H^\pm \to \tau\nu$ searches).

The exclusion contours of six direct searches in the $hMSSM$ scenario are displayed in Figure 3 (right). Note that the $hMSSM$ is only valid for $m_A > 130$ GeV. Those regions where even in this restricted parameter space the model is not strictly applicable are indicated by gray shaded regions in the figure. The exclusion contours of the (blue) $A/H/h \to \tau\tau$, (cyan) $A/H \to bb$ and (yellow) $A/H/h \to \mu\mu$ searches are comparable with those in the m_h^{mod+} scenario, while the $A/H/h \to \tau\tau$ search shows an extended and more continuous exclusion towards low $\tan\beta$ up for $m_A \lesssim 240$ GeV. The latter can be explained by a general shift of m_H to higher values relative to m_A for low $\tan\beta$, for which the analysis in turn is more sensitive. It turns out that the $H^\pm \to \tau\nu$ search has no sensitivity for $m_A > 130$ GeV due to the same shift of m_H, which is why it has not been added to the figure. On the other hand the searches for the $H \to hh$ and $A \to Zh$ decays gain sensitivity in the low $\tan\beta$ region for $m_A < 2m_t$. The exclusion by the combined search for the $H \to hh(bb\tau\tau)$ and $A \to Zh(\ell\ell\tau\tau)$ decay is shown in red. The exclusion contour obtained from the search of the $H \to hh(bb\gamma\gamma)$ decay is shown in green. They both cover a very similar region of the parameter space. Finally also indicated in the figure are the exclusion from the high mass $H \to WW/ZZ$ analysis, in orange, and the

constraint based on the compatibility with the observed couplings of the H^0 as discussed in Section 3, in magenta.

The figure demonstrates the exclusion of additional Higgs bosons next to the H^0 in the context of the $hMSSM$ for $m_A \lesssim 300$ GeV. This exclusion is driven by the $A/H/h \to \tau\tau$ search for large values of $\tan\beta$, the $H \to hh$ and $A \to Zh$ searches for low values of $\tan\beta$ and the couplings constraint in the intermediate range.

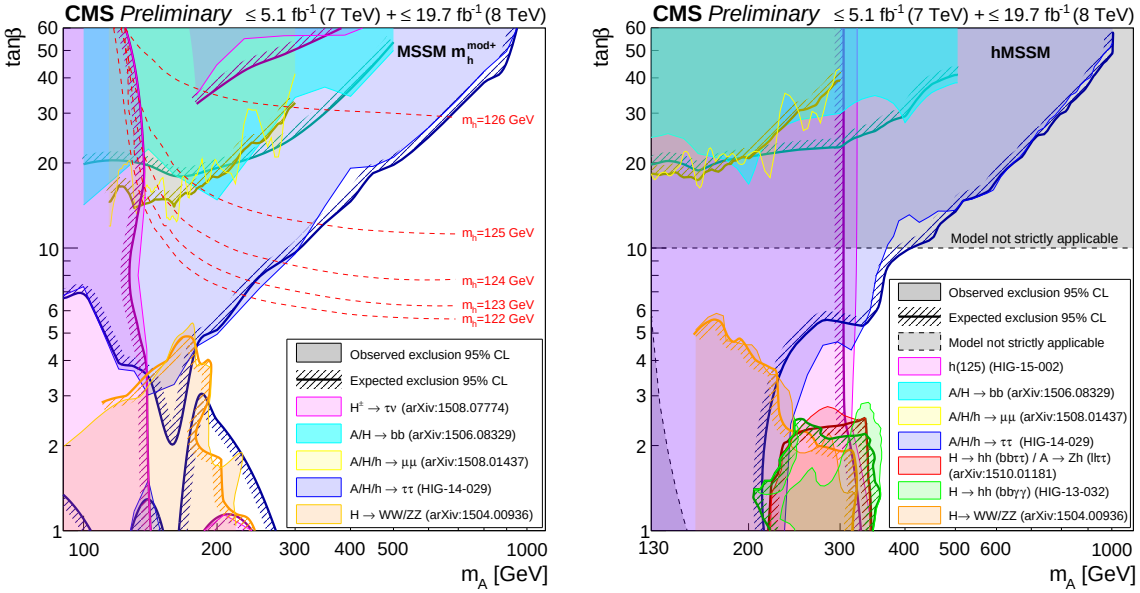

Figure 3: 95% CL exclusion contours, in the (left) MSSM m_h^{mod+} scenario (with $\mu = +200$ GeV) [30] and (right) $hMSSM$ [31, 32], as obtained by selected CMS analyses that have been performed on the LHC run-1 dataset. The exclusion contours for all direct searches have been determined as CL_S limits or re-interpreted from such limits. The colored filled areas correspond to the excluded regions in m_A and $\tan\beta$. The colored (slightly darker shaded) lines with indicated hatches to the regions that were expected to be excluded, based on the null-hypothesis assumption of a SM-like Higgs sector. Those regions in m_A and $\tan\beta$, where the $hMSSM$ is not strictly applicable are marked in gray. In the figure on the right in addition to the direct exclusion contours the constraint is displayed that is obtained from the compatibility of the scenario with the couplings of the H^0. This constraint has been obtained from an increase of the test statistic, $q(m_A, \tan\beta)$, as defined in the text by $\Delta q = 5.99$, corresponding to a 95% confidence region of a χ^2 function for two degrees of freedom.

5 Conclusions

The LHC run-1 data taking period has not only witnessed the search for the SM Higgs boson, resulting in the observation of a new particle, H^0 with a mass of 125.09 GeV, compatible with the expectations for the SM Higgs boson. But it has also witnessed a rich program of searches for Higgs bosons in the context of models beyond the SM. A prominent class of such models are the 2HDM and the MSSM as a special case of a 2HDM of *type*-II. For these models summary plots of a selected subset of analyses have been presented in four scenarios: one customized 2HDM scenario of *type*-I and one of *type*-II, the MSSM m_h^{mod+} and the $hMSSM$ scenario. In all scenarios the H^0 has been interpreted as the h.

In conclusion the 2HDM of *type*-I is generally constrained to $\cos(\beta - \alpha) \lesssim 0.5$ by the couplings

of the H^0 and the leading order relations between the angles α and β. In the chosen scenario it is further excluded at 95% CL for values of $m_H < 380$ GeV and $\tan\beta \lesssim 2$, driven by the re-interpretation of a search for an additional heavy Higgs boson in the WW and ZZ final state. The 2HDM of *type*-II is generally constrained to $\cos(\beta-\alpha) \lesssim 0.2$ for all $\tan\beta$ and for mass scales of the heavy Higgs bosons up to $\approx$ 380 GeV, with a small unconstrained corridor at $\tan\beta \approx 2$. In this scenario the exclusion is again driven by the $H \to WW/ZZ$ search, and by the constraints imposed by the couplings of the H^0. The exclusion of additional heavy Higgs bosons up to $\approx$ 300 GeV is also observed for the more specific MSSM scenarios. Here the exclusion is driven by the coupling constraints (in the $hMSSM$), a combined search for the $H \to hh(bb\tau\tau)$ and $A \to Zh(\ell\ell\tau\tau)$ decay and the re-interpretation of a search in the $H \to WW/ZZ$ decay channel at low values of $\tan\beta$ and the $A/H/h \to \tau\tau$ search at high values of $\tan\beta$.

Acknowledgments

We congratulate our colleagues in the CERN accelerator departments for the excellent performance of the LHC and thank the technical and administrative staffs at CERN and at other CMS institutes for their contributions to the success of the CMS effort. In addition, we gratefully acknowledge the computing centers and personnel of the Worldwide LHC Computing Grid for delivering so effectively the computing infrastructure essential to our analyses. Finally, we acknowledge the enduring support for the construction and operation of the LHC and the CMS detector provided by the following funding agencies: the Austrian Federal Ministry of Science, Research and Economy and the Austrian Science Fund; the Belgian Fonds de la Recherche Scientifique, and Fonds voor Wetenschappelijk Onderzoek; the Brazilian Funding Agencies (CNPq, CAPES, FAPERJ, and FAPESP); the Bulgarian Ministry of Education and Science; CERN; the Chinese Academy of Sciences, Ministry of Science and Technology, and National Natural Science Foundation of China; the Colombian Funding Agency (COLCIENCIAS); the Croatian Ministry of Science, Education and Sport, and the Croatian Science Foundation; the Research Promotion Foundation, Cyprus; the Ministry of Education and Research, Estonian Research Council via IUT23-4 and IUT23-6 and European Regional Development Fund, Estonia; the Academy of Finland, Finnish Ministry of Education and Culture, and Helsinki Institute of Physics; the Institut National de Physique Nucléaire et de Physique des Particules / CNRS, and Commissariat à l'Énergie Atomique et aux Énergies Alternatives / CEA, France; the Bundesministerium für Bildung und Forschung, Deutsche Forschungsgemeinschaft, and Helmholtz-Gemeinschaft Deutscher Forschungszentren, Germany; the General Secretariat for Research and Technology, Greece; the National Scientific Research Foundation, and National Innovation Office, Hungary; the Department of Atomic Energy and the Department of Science and Technology, India; the Institute for Studies in Theoretical Physics and Mathematics, Iran; the Science Foundation, Ireland; the Istituto Nazionale di Fisica Nucleare, Italy; the Ministry of Science, ICT and Future Planning, and National Research Foundation (NRF), Republic of Korea; the Lithuanian Academy of Sciences; the Ministry of Education, and University of Malaya (Malaysia); the Mexican Funding Agencies (CINVESTAV, CONACYT, SEP, and UASLP-FAI); the Ministry of Business, Innovation and Employment, New Zealand; the Pakistan Atomic Energy Commission; the Ministry of Science and Higher Education and the National Science Centre, Poland; the Fundação para a Ciência e a Tecnologia, Portugal; JINR, Dubna; the Ministry of Education and Science of the Russian Federation, the Federal Agency of Atomic Energy of the Russian Federation, Russian Academy of Sciences, and the Russian Foundation for Basic Research; the Ministry of Education, Science and Technological Development of Serbia; the Secretaría de Estado de Investigación, Desarrollo e Innovación and Programa

Consolider-Ingenio 2010, Spain; the Swiss Funding Agencies (ETH Board, ETH Zurich, PSI, SNF, UniZH, Canton Zurich, and SER); the Ministry of Science and Technology, Taipei; the Thailand Center of Excellence in Physics, the Institute for the Promotion of Teaching Science and Technology of Thailand, Special Task Force for Activating Research and the National Science and Technology Development Agency of Thailand; the Scientific and Technical Research Council of Turkey, and Turkish Atomic Energy Authority; the National Academy of Sciences of Ukraine, and State Fund for Fundamental Researches, Ukraine; the Science and Technology Facilities Council, UK; the US Department of Energy, and the US National Science Foundation.

Individuals have received support from the Marie-Curie program and the European Research Council and EPLANET (European Union); the Leventis Foundation; the A. P. Sloan Foundation; the Alexander von Humboldt Foundation; the Belgian Federal Science Policy Office; the Fonds pour la Formation à la Recherche dans l'Industrie et dans l'Agriculture (FRIA-Belgium); the Agentschap voor Innovatie door Wetenschap en Technologie (IWT-Belgium); the Ministry of Education, Youth and Sports (MEYS) of the Czech Republic; the Council of Science and Industrial Research, India; the HOMING PLUS program of Foundation for Polish Science, cofinanced from European Union, Regional Development Fund; the Compagnia di San Paolo (Torino); the Consorzio per la Fisica (Trieste); MIUR project 20108T4XTM (Italy); the Thalis and Aristeia programs cofinanced by EU-ESF and the Greek NSRF; and the National Priorities Research Program by Qatar National Research Fund.

References

[1] ATLAS Collaboration, "Observation of a new particle in the search for the Standard Model Higgs boson with the ATLAS detector at the LHC", *Phys. Lett.* **B716** (2012) 1–29, doi:10.1016/j.physletb.2012.08.020, arXiv:1207.7214.

[2] ATLAS Collaboration, "A particle consistent with the Higgs Boson observed with the ATLAS Detector at the Large Hadron Collider", *Science* **338** (2012) 1576–1582, doi:10.1126/science.1232005.

[3] CMS Collaboration, "Observation of a new boson with mass near 125 GeV in pp collisions at $\sqrt{s}$ = 7 and 8 TeV", *JHEP* **06** (2013) 081, doi:10.1007/JHEP06(2013)081, arXiv:1303.4571.

[4] CMS Collaboration, "A New Boson with a Mass of 125 GeV Observed with the CMS Experiment at the Large Hadron Collider", *Science* **338** (2012) 1569–1575, doi:10.1126/science.1230816.

[5] CMS Collaboration, "Observation of a new boson at a mass of 125 GeV with the CMS experiment at the LHC", *Phys. Lett.* **B716** (2012) 30–61, doi:10.1016/j.physletb.2012.08.021, arXiv:1207.7235.

[6] ATLAS Collaboration, "Measurements of Higgs boson production and couplings in the four-lepton channel in pp collisions at center-of-mass energies of 7 and 8 TeV with the ATLAS detector", *Phys. Rev.* **D91** (2015), no. 1, 012006, doi:10.1103/PhysRevD.91.012006, arXiv:1408.5191.

[7] CMS Collaboration, "Measurement of the properties of a Higgs boson in the four-lepton final state", *Phys. Rev.* **D89** (2014), no. 9, 092007, doi:10.1103/PhysRevD.89.092007, arXiv:1312.5353.

[8] ATLAS Collaboration, "Measurement of Higgs boson production in the diphoton decay channel in pp collisions at center-of-mass energies of 7 and 8 TeV with the ATLAS detector", *Phys. Rev.* **D90** (2014), no. 11, 112015, doi:10.1103/PhysRevD.90.112015, arXiv:1408.7084.

[9] CMS Collaboration, "Observation of the diphoton decay of the Higgs boson and measurement of its properties", *Eur. Phys. J.* **C74** (2014), no. 10, 3076, doi:10.1140/epjc/s10052-014-3076-z, arXiv:1407.0558.

[10] ATLAS Collaboration, "Observation and measurement of Higgs boson decays to WW* with the ATLAS detector", *Phys. Rev.* **D92** (2015), no. 1, 012006, doi:10.1103/PhysRevD.92.012006, arXiv:1412.2641.

[11] CMS Collaboration, "Measurement of Higgs boson production and properties in the WW decay channel with leptonic final states", *JHEP* **01** (2014) 096, doi:10.1007/JHEP01(2014)096, arXiv:1312.1129.

[12] ATLAS Collaboration, "Evidence for the Higgs-boson Yukawa coupling to tau leptons with the ATLAS detector", *JHEP* **04** (2015) 117, doi:10.1007/JHEP04(2015)117, arXiv:1501.04943.

[13] CMS Collaboration, "Evidence for the 125 GeV Higgs boson decaying to a pair of τ leptons", *JHEP* **05** (2014) 104, doi:10.1007/JHEP05(2014)104, arXiv:1401.5041.

[14] CMS Collaboration, "Evidence for the direct decay of the 125 GeV Higgs boson to fermions", *Nature Phys.* **10** (2014) 557–560, doi:10.1038/nphys3005, arXiv:1401.6527.

[15] ATLAS Collaboration, "Search for the Standard Model Higgs boson decay to $\mu^+\mu^-$ with the ATLAS detector", *Phys. Lett.* **B738** (2014) 68–86, doi:10.1016/j.physletb.2014.09.008, arXiv:1406.7663.

[16] CMS Collaboration, "Search for a standard model-like Higgs boson in the $\mu^+\mu$ and e^+e^- decay channels at the LHC", *Phys. Lett.* **B744** (2015) 184–207, doi:10.1016/j.physletb.2015.03.048, arXiv:1410.6679.

[17] ATLAS Collaboration, "Evidence for the spin-0 nature of the Higgs boson using ATLAS data", *Phys. Lett.* **B726** (2013) 120–144, doi:10.1016/j.physletb.2013.08.026, arXiv:1307.1432.

[18] CMS Collaboration, "Constraints on the spin-parity and anomalous HVV couplings of the Higgs boson in proton collisions at 7 and 8 TeV", *Phys. Rev.* **D92** (2015), no. 1, 012004, doi:10.1103/PhysRevD.92.012004, arXiv:1411.3441.

[19] ATLAS Collaboration, "Constraints on the off-shell Higgs boson signal strength in the high-mass ZZ and WW final states with the ATLAS detector", *Eur. Phys. J.* **C75** (2015), no. 7, 335, doi:10.1140/epjc/s10052-015-3542-2, arXiv:1503.01060.

[20] CMS Collaboration, "Constraints on the Higgs boson width from off-shell production and decay to Z-boson pairs", *Phys. Lett.* **B736** (2014) 64–85, doi:10.1016/j.physletb.2014.06.077, arXiv:1405.3455.

[21] CMS Collaboration, "Precise determination of the mass of the Higgs boson and tests of compatibility of its couplings with the standard model predictions using proton collisions at 7 and 8 TeV", *Eur. Phys. J.* **C75** (2015), no. 5, 212, doi:10.1140/epjc/s10052-015-3351-7, arXiv:1412.8662.

[22] ATLAS Collaboration, "Measurements of the Higgs boson production and decay rates and coupling strengths using pp collision data at $\sqrt{s} = 7$ and 8 TeV in the ATLAS experiment", *Eur. Phys. J.* **C76** (2016), no. 1, 6, doi:10.1140/epjc/s10052-015-3769-y, arXiv:1507.04548.

[23] CMS Collaboration, "Measurements of the Higgs boson production and decay rates and constraints on its couplings from a combined ATLAS and CMS analysis of the LHC pp collision data at $\sqrt{s}$ = 7 and 8 TeV", CMS Physics Analysis Summary CMS-PAS-HIG-15-002, 2015.

[24] ATLAS, CMS Collaboration, "Combined Measurement of the Higgs Boson Mass in pp Collisions at $\sqrt{s} = 7$ and 8 TeV with the ATLAS and CMS Experiments", *Phys. Rev. Lett.* **114** (2015) 191803, doi:10.1103/PhysRevLett.114.191803, arXiv:1503.07589.

[25] G. C. Dorsch, S. J. Huber, K. Mimasu, and J. M. No, "Echoes of the Electroweak Phase Transition: Discovering a second Higgs doublet through $A_0 \to ZH_0$", *Phys. Rev. Lett.* **113** (2014), no. 21, 211802, doi:10.1103/PhysRevLett.113.211802, arXiv:1405.5537.

[26] H. Haber and O. Stal, "New LHC benchmarks for the CP-conserving two-Higgs-doublet model", *Eur. Phys. J.* **C75** (2015) 491, doi:10.1140/epjc/s10052-015-3697-x, arXiv:1507.04281.

[27] Particle Data Group Collaboration, "Review of Particle Physics", *Chin.Phys.* **C38** (2014) 090001, doi:10.1088/1674-1137/38/9/090001.

[28] R. V. Harlander, S. Liebler, and H. Mantler, "SusHi: A program for the calculation of Higgs production in gluon fusion and bottom-quark annihilation in the Standard Model and the MSSM", *Comput. Phys. Commun.* **184** (2013) 1605–1617, doi:10.1016/j.cpc.2013.02.006, arXiv:1212.3249.

[29] D. Eriksson, J. Rathsman, and O. Stal, "2HDMC: Two-Higgs-Doublet Model Calculator Physics and Manual", *Comput. Phys. Commun.* **181** (2010) 189–205, doi:10.1016/j.cpc.2009.09.011, arXiv:0902.0851.

[30] P. Bechtle et al., "Probing the Standard Model with Higgs signal rates from the Tevatron, the LHC and a future ILC", *JHEP* **11** (2014) 039, doi:10.1007/JHEP11(2014)039, arXiv:1403.1582.

[31] A. Djouadi et al., "The post-Higgs MSSM scenario: Habemus MSSM?", *Eur. Phys. J.* **C73** (2013) 2650, doi:10.1140/epjc/s10052-013-2650-0, arXiv:1307.5205.

[32] A. Djouadi et al., "Fully covering the MSSM Higgs sector at the LHC", *JHEP* **06** (2015) 168, doi:10.1007/JHEP06(2015)168, arXiv:1502.05653.

[33] G. Degrassi et al., "Towards high precision predictions for the MSSM Higgs sector", *Eur. Phys. J.* **C28** (2003) 133–143, doi:10.1140/epjc/s2003-01152-2, arXiv:hep-ph/0212020.

[34] LHCHXSWG Collaboration, "Benchmark scenarios for low tan β in the MSSM", public note LHCHXSWG-2015-002, 2015.

[35] LHC Higgs Cross Section Working Group et al., "Handbook of LHC Higgs Cross Sections: 3. Higgs Properties", *CERN-2013-004* (CERN, Geneva, 2013) arXiv:1307.1347.

[36] T. Junk, "Confidence level computation for combining searches with small statistics", *Nucl. Instrum. Meth.* **A434** (1999) 435–443, doi:10.1016/S0168-9002(99)00498-2, arXiv:hep-ex/9902006.

[37] A. L. Read, "Presentation of search results: The CL(s) technique", *J. Phys.* **G28** (2002) 2693–2704, doi:10.1088/0954-3899/28/10/313.

[38] CMS Collaboration, "Search for additional neutral Higgs bosons decaying to a pair of tau leptons in pp collisions at $\sqrt{s} = 7$ and 8 TeV", CMS Physics Analysis Summary CMS-PAS-HIG-14-029, 2015.

[39] L. Bianchini, J. Conway, E. K. Friis, and C. Veelken, "Reconstruction of the Higgs mass in $H \to \tau\tau$ Events by Dynamical Likelihood techniques", *J.Phys.Conf.Ser.* **513** (2014) 022035, doi:10.1088/1742-6596/513/2/022035.

[40] T. Sjöstrand, S. Mrenna, and P. Skands, "PYTHIA 6.4 physics and manual", *JHEP* **05** (2006) 026, doi:10.1088/1126-6708/2006/05/026, arXiv:hep-ph/0603175.

[41] A. L. Read, "Linear interpolation of histograms", *Nucl. Instrum. Meth.* **A425** (1999) 357–360, doi:10.1016/S0168-9002(98)01347-3.

[42] CMS Collaboration, "Search for neutral MSSM Higgs bosons decaying to $\mu^+\mu^-$ in pp collisions at $\sqrt{s} = 7$ and 8 TeV", *Phys. Lett.* **B752** (2016) 221–246, doi:10.1016/j.physletb.2015.11.042, arXiv:1508.01437.

[43] T. Hahn et al., "High-Precision Predictions for the Light CP -Even Higgs Boson Mass of the Minimal Supersymmetric Standard Model", *Phys. Rev. Lett.* **112** (2014), no. 14, 141801, doi:10.1103/PhysRevLett.112.141801, arXiv:1312.4937.

[44] M. Frank et al., "The Higgs Boson Masses and Mixings of the Complex MSSM in the Feynman-Diagrammatic Approach", *JHEP* **02** (2007) 047, doi:10.1088/1126-6708/2007/02/047, arXiv:hep-ph/0611326.

[45] S. Heinemeyer, W. Hollik, and G. Weiglein, "The Masses of the neutral CP - even Higgs bosons in the MSSM: Accurate analysis at the two loop level", *Eur. Phys. J.* **C9** (1999) 343–366, doi:10.1007/s100529900006, arXiv:hep-ph/9812472.

[46] S. Heinemeyer, W. Hollik, and G. Weiglein, "FeynHiggs: A Program for the calculation of the masses of the neutral CP even Higgs bosons in the MSSM", *Comput. Phys. Commun.* **124** (2000) 76–89, doi:10.1016/S0010-4655(99)00364-1, arXiv:hep-ph/9812320.

[47] CMS Collaboration, "Search for Neutral MSSM Higgs Bosons Decaying into A Pair of Bottom Quarks", *JHEP* **11** (2015) 071, doi:10.1007/JHEP11(2015)071, arXiv:1506.08329.

[48] CMS Collaboration, "Search for a charged Higgs boson in pp collisions at $\sqrt{s} = 8$ TeV", *JHEP* **11** (2015) 018, doi:10.1007/JHEP11(2015)018, arXiv:1508.07774.

[49] CMS Collaboration, "Searches for a heavy scalar boson H decaying to a pair of 125 GeV Higgs bosons hh or for a heavy pseudoscalar boson A decaying to Zh, in the final states with h to tautau", *Phys. Lett.* **B755** (2016) 217–244, doi:10.1016/j.physletb.2016.01.056, arXiv:1510.01181.

[50] CMS Collaboration, "Search for the resonant production of two Higgs bosons in the final state with two photons and two bottom quarks", CMS Physics Analysis Summary CMS-PAS-HIG-13-032, 2014.

[51] CMS Collaboration, "Search for a Higgs Boson in the Mass Range from 145 to 1000 GeV Decaying to a Pair of W or Z Bosons", *JHEP* **10** (2015) 144, doi:10.1007/JHEP10(2015)144, arXiv:1504.00936.

[52] CMS Collaboration, "Search for H/A decaying into Z+A/H, with Z to ll and A/H to fermion pair", CMS Physics Analysis Summary CMS-PAS-HIG-15-001, 2015.